CHAPTER 4

RESULTS AND DISCUSSION

Characterization of starting materials

The appearance of RHA silica obtained from burning acid-leached RH and unleached RH at different temperatures is shown in Fig. 4.1 and Fig. 4.2, respectively. It is clearly seen that the change in colour of samples is relative to burning temperatures. The whiteness of the obtained RHA silica increased with increase in burning temperature due to the removal of carbon in the RH. The RHA silica samples from the acid-leached RH obtained at low temperatures of 400 °C and 500 °C are black and brown in colour, respectively, whilst with higher temperature of 600 °C grayish-white RHA silica was obtained. However, the RHA silica white in colour is obtained after burning the acid-leached RH at 700-900 °C. The XRD results shown in Fig. 4.3 reveal that all of the samples obtained from acid-leached RH are of amorphous phase with a board peak centered around 22.2° (2θ). In spite of the high temperatures of 800 °C and 900 °C employed in this experiment, the structure of silica presented in the ash remains amorphous, and no traces of crystalline phase are observed at the diffraction peaks of 21.7° and 20.6° (2θ), which are assigned to cristobalite and tridymite silica, respectively. According to other reports[1, 16, 47, 48, 76], burning the RH at high temperatures (>700 °C) led to the crystallization of amorphous silica to cristobalite and tridymite. These reports are in contrast to the results obtained. In addition to burning temperature, reaction time, reheating the ash to remove unburned carbon, the alkali content, especially K_2O and Na_2O, presented in the RH is also an important factor that influences the phase transformation of silica. From Table 4.1, it is noticed that much of the K_2O was removed from RH by acid leaching. It is possible that the K_2O content remaining in acid-leached RH is not enough to accelerate the crystallization of the amorphous silica. From Table 4.2, the specific surface area is found to be 240 m^2/g for the sample obtained at 700 °C and begins to decrease considerably after burning at 800 °C due to agglomeration effect, hence diminishing pososity[1].

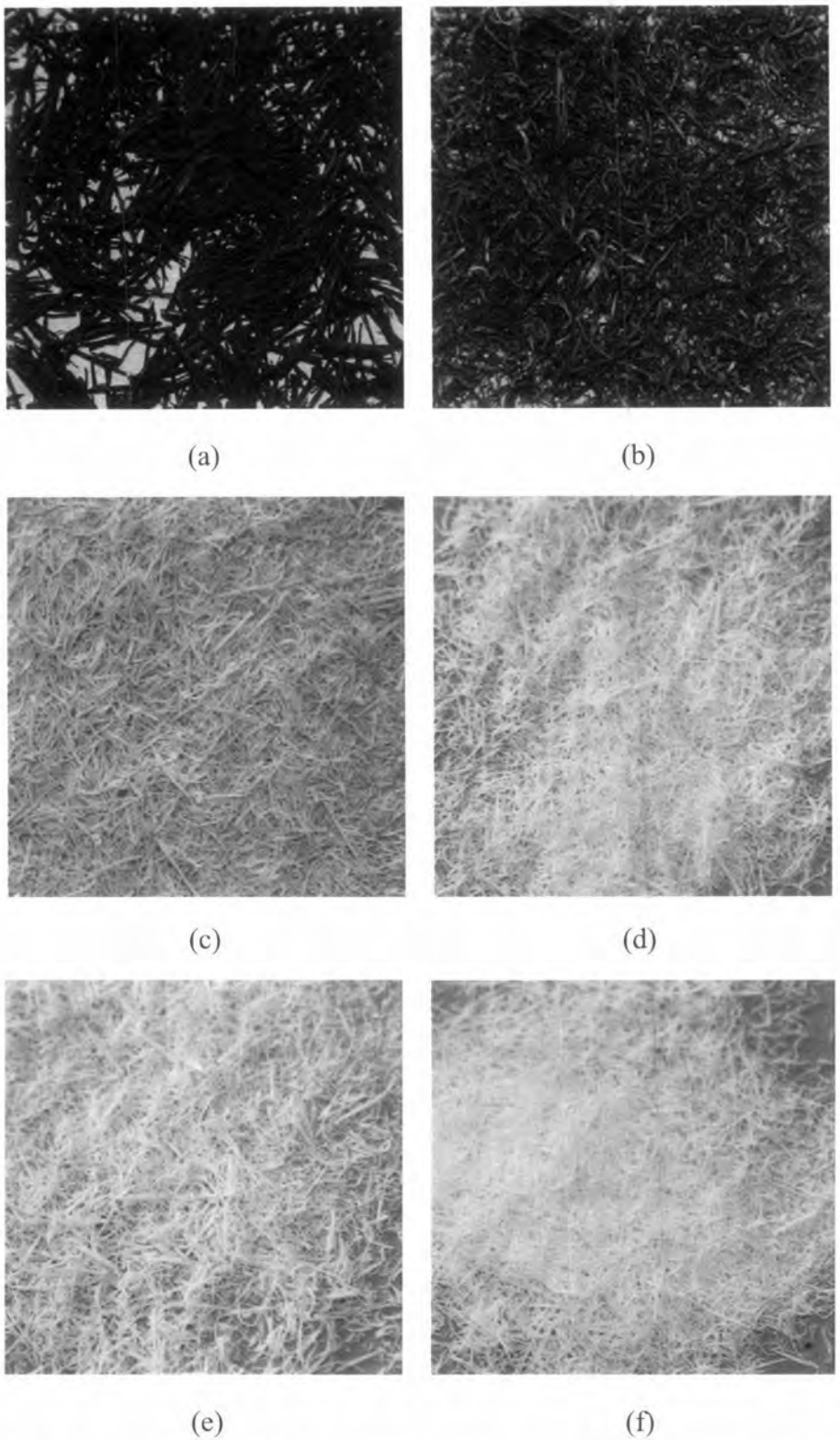

Fig. 4.1 Photographs of acid-leached RHA silica obtained at (a) 400 °C, (b) 500 °C, (c) 600 °C, (d) 700 °C, (e) 800 °C and (f) 900 °C.

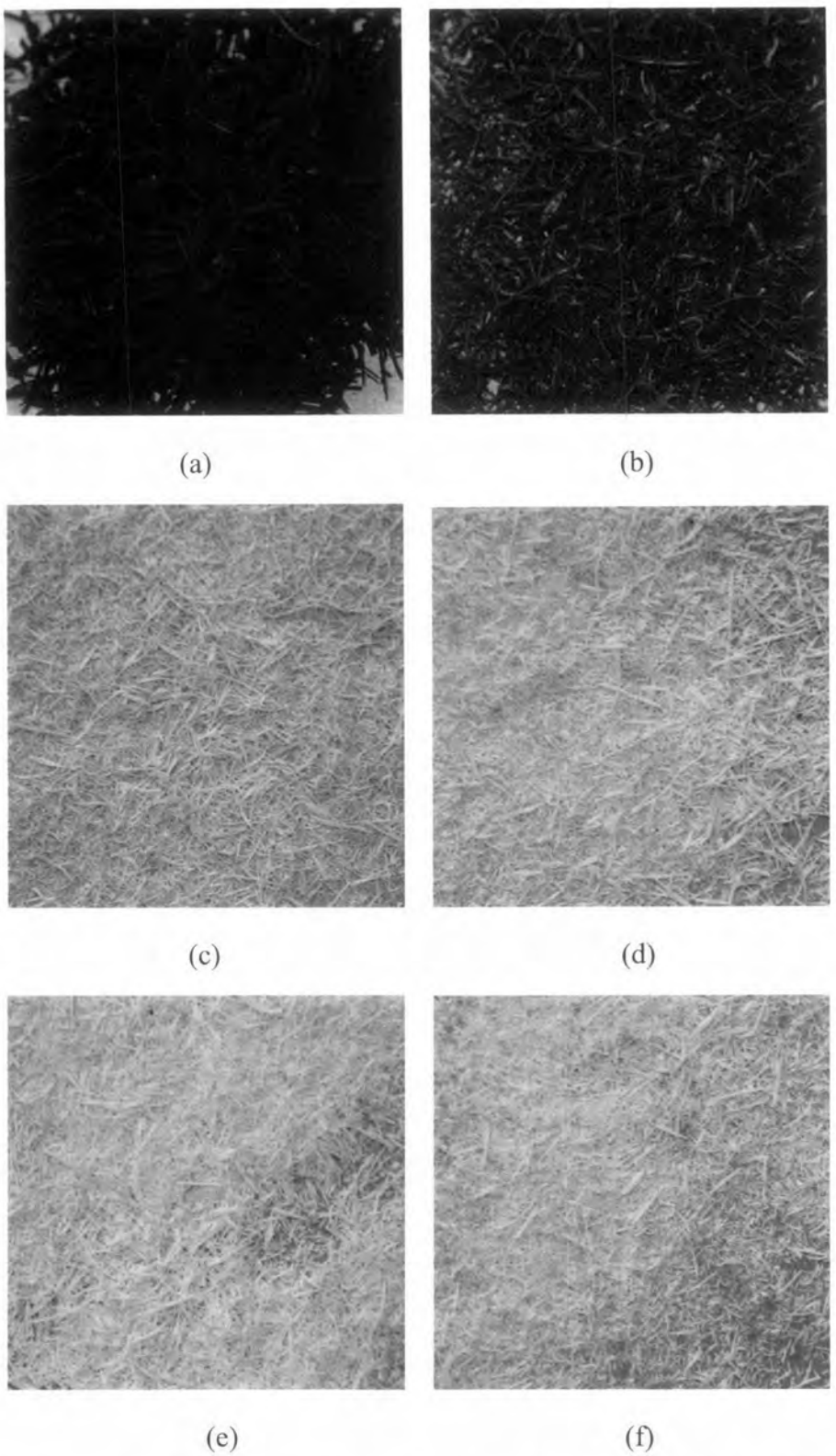

Fig. 4.2 Photographs of unleached RHA silica obtained at (a) 400 °C, (b) 500 °C, (c) 600 °C, (d) 700 °C, (e) 800 °C and (f) 900 °C.

Many researchers have concluded that preliminary leaching of RH with acid solution before thermal treatment produces high purity RHA silica with completely white colour and high specific surface area. According to Krishnarao et al., when RH was subjected to acid treatment, the cellulose which formed the main body of RH was reduced and carbohydrate was blackened due to removal of oxygen. The proteins in the RH were decomposed into amino acids, and the cellulose of larger molecular weight was leached out as smaller molecular weight compounds. For this reason, the leaching of rice husk with HCl acid solution before its burning eases the decompose of the organic matter into carbon, which can be generally oxidized with increase in temperature.

Table 4.1 The chemical analysis (XRF) and BET surface area of RHA silica obtained at 700 °C for 3 h.

Chemical composition	Sample (wt %)	
	Acid-leached RH	Unleached RH**
SiO_2	99.64	96.10
Al_2O_3	0.08	0.06
Na_2O	0.00	0.21
K_2O	0.04	0.76
P_2O_5	0.10	0.42
CaO	0.04	1.21
SO_3	0.03	0.50
Fe_2O_3	0.04	0.12
CuO	0.01	0.01
MoO_3	0.01	0.01
ZnO	-	0.02
MnO	-	0.08
MgO	-	0.08
Others	0.03	0.04
Wt. loss*	$4x10^{-3}$	0.38
SiO_2/Al_2O_3 molar ratio	2075	2667
Ash color	White	Greyish-white
BET surface area (m^2/g)	240	102

*Calcined at 1000 C for 3 h.

**Sample was treated by boiling rice husk with distilled water for 2 h.

Table 4.2 Mineral phase and BET surface area of the RHA silica obtained from different conditions

Sample	Phased formed	BET surface area (m^2/g)	Ash colour
Acid-leached RH			
400 °C	Amorphous	83	Black
500 °C	Amorphous	198	Brown
600 °C	Amorphous	229	Grayish-white
700 °C	Amorphous	240	White
800 °C	Amorphous	160	White
900 °C	Amorphous	58	White
Unleached RH			
700 °C	Amorphous	102	Grayish-white
800 °C	Amorphous	33	Grayish-white
900 °C	Amorphous	12	Grayish-white

To confirm the report of Krishnarao[48], RH was also treated by boiling rice husk with distilled water for 2 h. Table 4.1 shows chemical and physical properties of the RHA silica obtained from different methods. It is observed that the acid leaching treatment is very effective for removing most of the metallic impurities in rice husk, resulting in a white RHA with high purity silica (99.6 %) and high specific surface area (240 m^2/g), whilst a slightly grayish-white sample (Fig. 4.2 (d)) obtained from unleached RH (boiled RH with distilled water) contains lower silica content (96.1 %) and lower specific surface area (102 m^2/g). The slightly grayish-white specks appearing in some particles of unleached RHA silica was due to the retained carbon or unoxidized carbon[48], leading to decrease in the specific surface area. The SEM micrographs (Fig. 4.4) reveal that the morphologies of RHA silica obtained from unleached RH and acid-leached RH are similar, but different in size. They have an irregular geometry and a smooth surface in opposite direction. Average particle sizes of the unleached and acid-leached RHA silica are 100 μm and 50 μm, respectively. A coarser particle size of the unleached RHA silica is probably resulted from incomplete burning of the RH. Although the unleached RH is

burnt at high temperatures of 800 °C and 900 °C, the colour of the obtained RHA silica is not much different from that of 700 °C, as shown in Fig. 4.2, but the specific surface area is considerably decreased. The XRD results shown in Fig. 4.5 clearly reveal that all of samples are also amorphous silica regardless of the heating temperatures and alkali contents (Table 4.1). This implies that simply boiling the RH with water prior to calcining effectively reduces the alkali content below the critical limit that induces the phase transformation. In addition to the agglomeration effect at high temperatures, the decrease in the specific surface area of the unleached RHA silica obtained at 800 °C and 900 °C is probably due to the surface melting of silica. This finding agrees well with the report of Krishnarao et al.[48] that, above 800 °C, K_2O dissociated to form K^+ which strongly interacted with silica in the RHA and caused surface melting, leading to the carbon fixation.

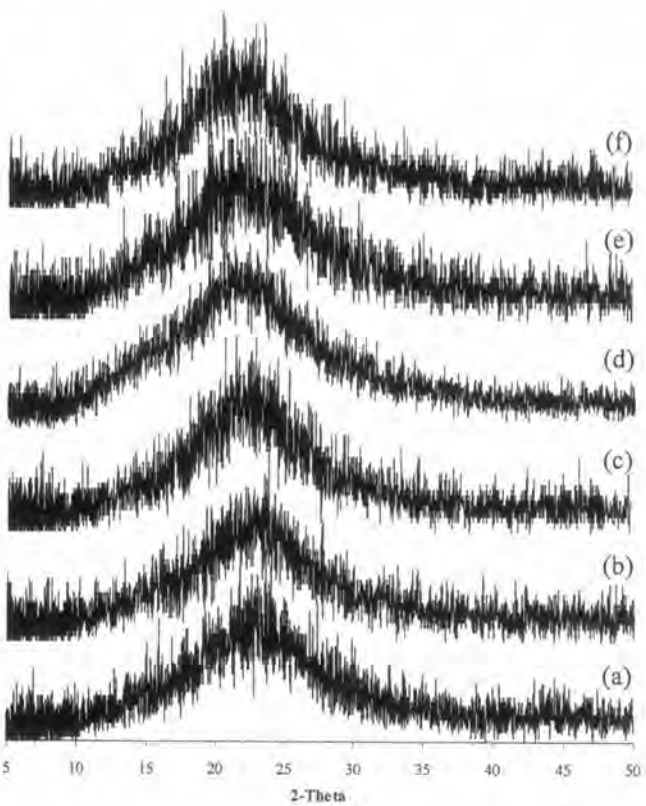

Fig. 4.3 Representative XRD patterns of RHA silica obtained from burning acid-leached RH at different temperatures. XRD derived diffractograms obtained from (a) 400 °C, (b) 500 °C, (c) 600 °C, (d) 700 °C, (e) 800 °C and (f) 900 °C.

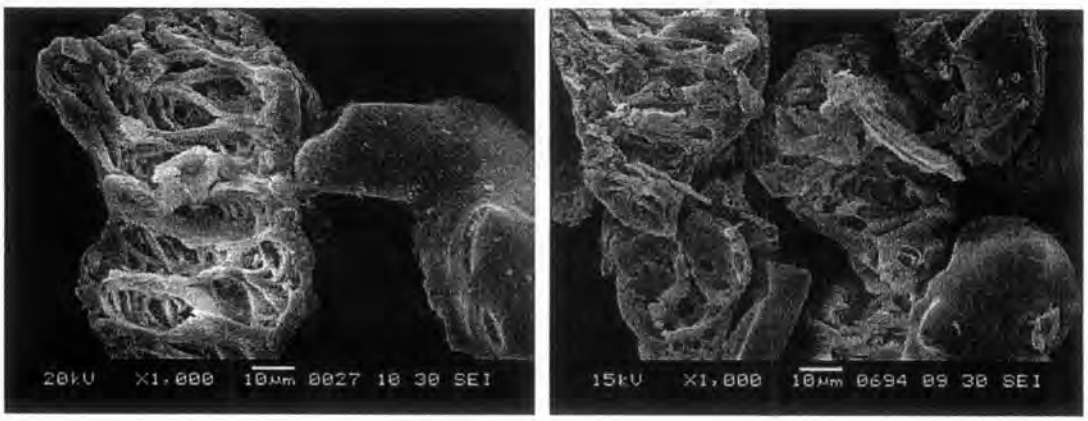

(a) (b)

Fig. 4.4 Representative SEM micrographs of (a) unleached RHA silica, and (b) acid-leached RHA silica obtained by burning at 700 °C for 3 h.

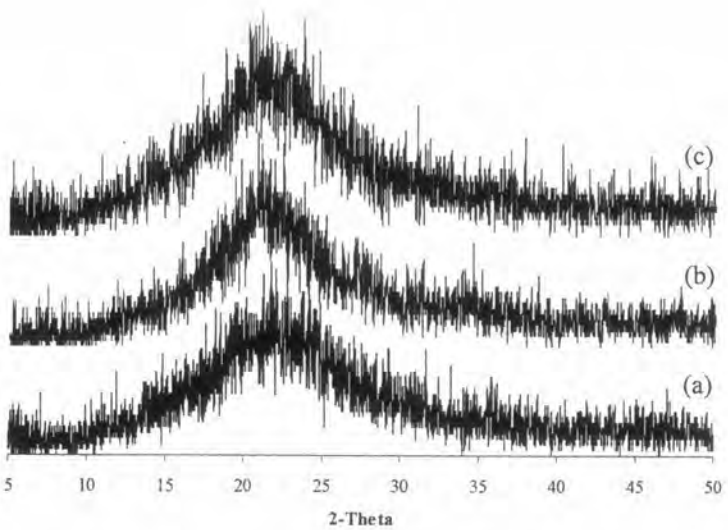

Fig. 4.5 Representative XRD patterns of RHA silica obtained from burning unleached RH at (a) 700 °C and (b) 800 °C and (c) 900 °C.

Characterization of the products

A. Preliminary experiments

Preliminary experiments were carried out in order to establish the optimum synthesis conditions for ZSM-5, using acid-leached RHA obtained at 700 °C as silica source. The synthesis was performed at SiO_2/Al_2O_3 molar ratio of 80 by hydrothermal treatment (150 °C, 48 h), using 2 g RHA silica and 0.9 mol/l TPABr as the organic template. The results were obtained as follows:

1. Effect of RHA silica obtained from different precleaning methods

Fig. 4.6 shows the XRD results of the product obtained from different RHA silica. It was observed that a single phase of ZSM-5 with a high crystallinity was produced from acid-leached RHA silica, whilst poorly crystalline ZSM-5 and amorphous phase were produced from unleached RHA silica at the same synthesis time (48 h). It has been well known that silica in an amorphous form is a highly active reactant in the zeolite synthesis because it readily dissolves in the alkali solution to form a precursor gel which leads to the quick crystallization of pure zeolite, whilst crystalline silica is inactive[9]. Though both types of RHA silica (leached and unleached) used as the starting materials in the present synthesis of ZSM-5 were in amorphous form, they showed relatively different formation of ZSM-5 zeolite. Mohamed et al.[6] reported that nucleation and crystallization rates depended on the dissolution of the silica precursor. Due to its high specific surface area, therefore, it can be said that the aicd-leached RHA silica was effectively dissolved in alkaline NaOH solution, leading to a better crystallization. To complete the crystallization of ZSM-5, the precursor gel prepared from the unleached RHA silica was hydrothermally synthesized with extended reaction times. It was found that a highly crystalline ZSM-5 was obtained a reaction time of 96 h.

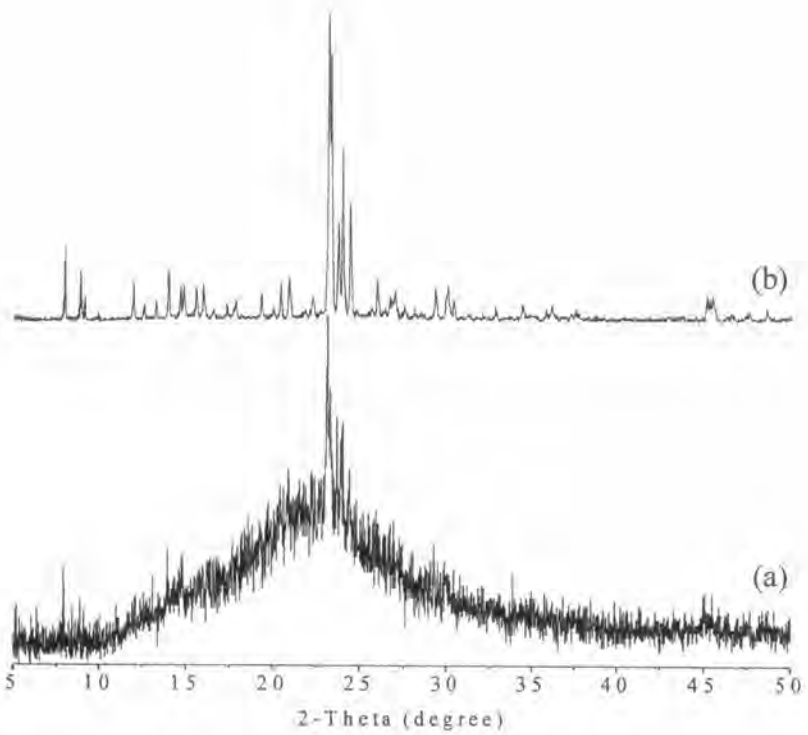

Fig. 4.6 Representative XRD patterns of as-synthesized samples obtained at SiO_2/Al_2O_3 molar ratio of 80 using (a) unleached-RHA and (b) acid-leached RHA silica.

2. Effect of ground RHA silica

For the production of ZSM-5, the use of TPABr as organic template is a common practice. This organic agent is required for the formation of ZSM-5 crystal structure. Although, TPABr organic template is effective to the synthesis of ZSM-5 it can cause a high production cost and air pollution, resulting from thermal decomposition of organic molecules trapped in the pore of ZSM-5 crystals. In order to reduce these problems, the ground acid-leached RHA silica was employed in this experiment. However, due to the strong agglomeration of the ground RHA, its average particle size had to be estimated from the SEM micrographs, an example of which is shown in Fig. 4.7. An average

particle size of ground RHA silica was around 0.1 μm which had a finer particle size than that of as-prepared RHA silica (~50 μm).

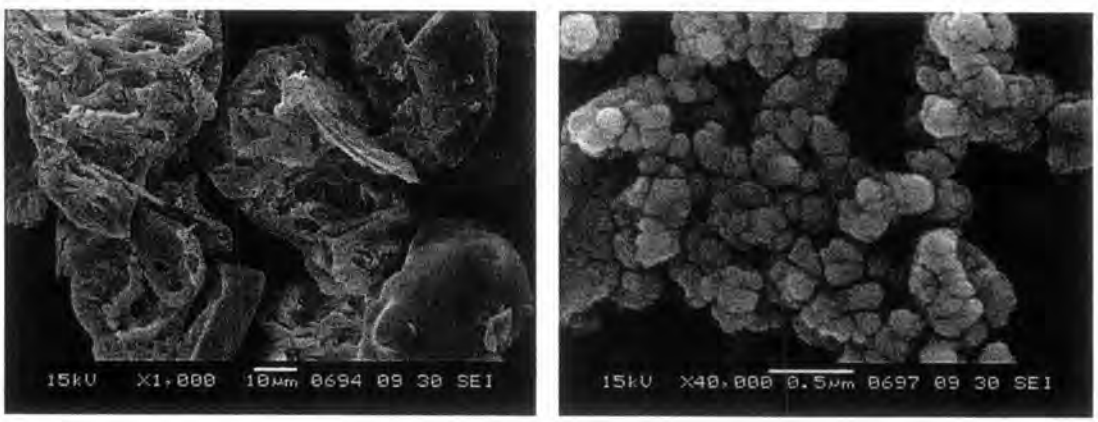

(a) (b)

Fig. 4.7 Representative SEM micrographs of (a) as-prepared RHA silica grains, and (b) agglomerates of ground RHA silica.

Fig. 4.8 shows the XRD results of as-synthesized ZSM-5 obtained at SiO_2/Al_2O_3 molar ratio of 80. It was found that the ground RHA silica used as starting material could reduce both the TPABr content and the synthesis time. However, it was quite difficult to produce ZSM-5 without TPABr organic template. When using the ground RHA silica without TPABr organic template (Fig. 4.8 (a)), no trace of ZSM-5 zeolite was observed at the diffraction peaks in the ranges of 2θ= 7-9° and 2θ=23-25°. The well crystalline ZSM-5 was able to be produced from the ground RHA silica in a short synthesis time (24 h) and at a low concentration of TPABr (0.18 mol/L). A dramatic improvement was due to the high dissolution of silica. A finer particle enhanced the dissolution of RHA silica in alkali medium, leading to increase in crystallization rate.

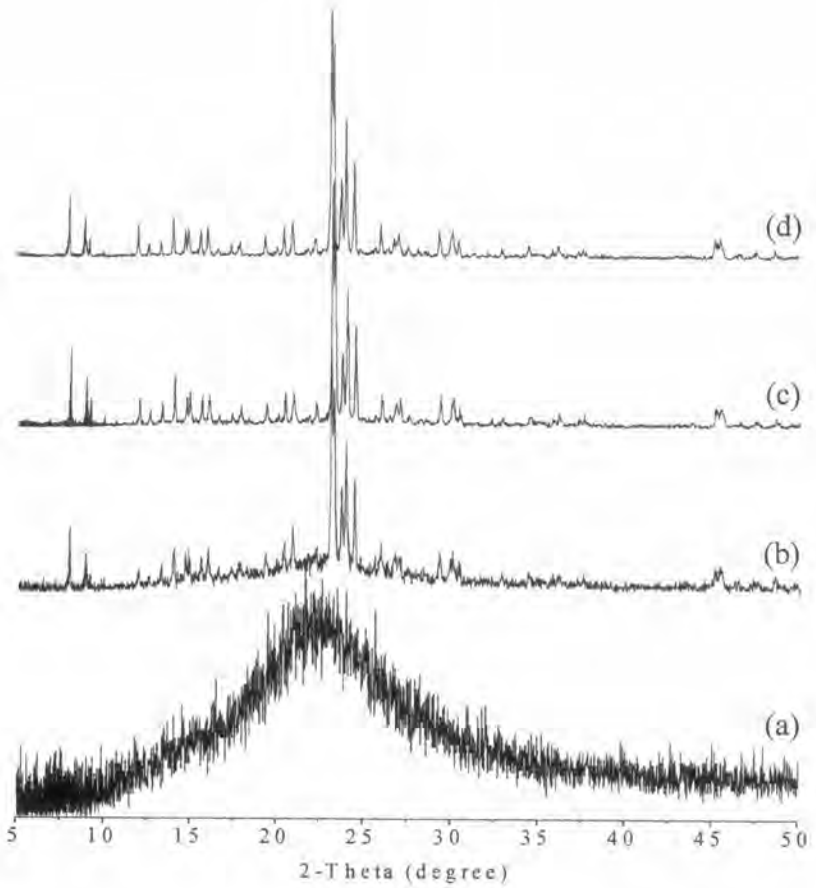

Fig. 4.8 Representative XRD patterns of as-synthesized samples obtained from

(a) ground RHA silica without TPABr, 48 h

(b) ground RHA silica with 0.18 TPABr, 20 h

(c) ground RHA silica with 0.18 TPABr, 24 h and

(d) as-prepared RHA silica with 0.9 mol/L TPABr, 48 h.

B. Synthesis of ZSM-5 zeolite and silicalite

From preliminary experiments, using a stainless steel bomb lined with PTFE under autogenous pressure at different SiO_2/Al_2O_3 molar ratios, a well crystalline ZSM-5 was obtained at a SiO_2/Al_2O_3 molar ratio of 80 under hydrolysis at 150 C for 48 h, using 0.9 mol/L TPABr as the organic template. Moreover, when using ground RHA silica, ZSM-5 with high crystallinity could be obtained at the same temperature in only 24 h without increasing the template content. Therefore, in this study ground RHA silica and a reduced template concentration were employed to reduce the organic template content and the reaction time.

Table 4.3 The chemical composition and mineral phase of ZSM-5zeolite and silicalite

SiO_2/Al_2O_3 molar ratio in the gel	SiO_2/Al_2O_3 molar ratio in the zeolite	Synthesis time (h)	Phase formed	Synthesis yield** (%)
30	n.d.	120	Amorphous, ZSM-5*	n.d.
50	n.d.	72	Amorphous, ZSM-5*	n.d.
80	120	24	ZSM-5 zeolite	84.1 ± 0.49
100	157	12	ZSM-5 zeolite	71.8 ± 0.74
200	163	12	ZSM-5 zeolite	70.2 ± 1.79
400	Only SiO_2	6	Silicalite	60.1 ± 0.65
800	Only SiO_2	6	Silicalite	57.8 ± 0.89
1000	Only SiO_2	4	Silicalite	56.9 ± 1.00
2075	Only SiO_2	4	Silicalite	56.8 ± 1.08

n.d. = not determined

*Poorly crystalline ZSM-5 zeolite.

**Data for the % synthesis yield are the mean taken from 3 separated runs (95% confidence level).

Table 4.3 shows the chemical compositions, mineral phases, synthesis times and the yield of the products obtained at the optimized synthesis times. The range of synthesis times investigated in each experiment was determined according to the range of the SiO_2/Al_2O_3 molar ratio. That is for low SiO_2/Al_2O_3 molar ratios, of 80 or less, they were

assayed after 10, 12, 22, 24, 30 and 120 h; whist for higher SiO_2/Al_2O_3 molar ratios, of 100 and above, they were assayed after 2, 3, 4, 5, 6, 10 and 12 h. Since it is well known that the surface area, crystallinity and mineral phase of the hydrolysis product varies along the course of hydrothermal treatment[8] , the optimization is based on the conditions revealed by the XRD that first gave well crystalline ZSM-5 with no trace of the amorphous RHA silica (hump around 22° 2θ).

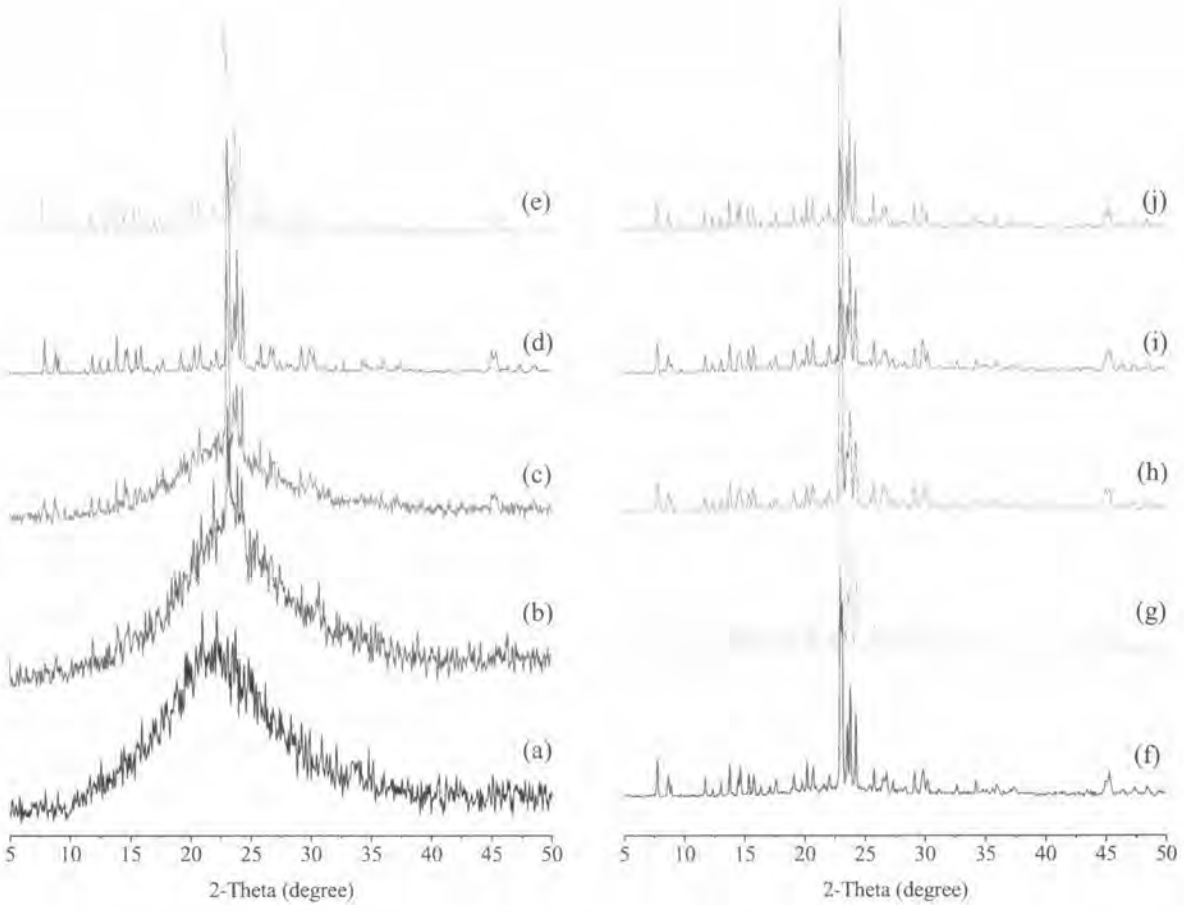

Fig. 4.9 Representative XRD patterns of as-synthesized samples obtained at different SiO_2/Al_2O_3 molar ratios. XRD derived diffractograms obtained from (a) RHA, and from SiO_2/Al_2O_3 molar ratios of (b) 30, (c) 50, (d) 80, (e) 100, (f) 200, (g) 400, (h) 800, (i) 1000 and (j) 2075.

The XRD results (Fig. 4.9) clearly revealed that the crystallinity of ZSM-5 increases with increasing SiO_2/Al_2O_3 molar ratios. SiO_2/Al_2O_3 molar ratios from 80 to 2075 produced a single phase of well crystalline ZSM-5 in a short time (24 - 4 h), whist SiO_2/Al_2O_3 molar ratios below 80 (i.e. 50 and 30), yield poorly crystalline ZSM-5 and an amorphous phase was principally formed instead. This finding agrees well with the report of Szostak[3] that the crystallization rate for the formation of ZSM-5 increased (i) as the aluminum content decreased, (ii) with a SiO_2/Al_2O_3 ratio above 100, and (iii) that the greater the NaOH concentration, the lower the yield of the crystalline material attained. Despite keeping the pH of each gel around 11 with the addition of HNO_3 in gel preparation, the total NaOH concentration of the gel varied depending on the content of $NaAlO_2$ added in order to set the SiO_2/Al_2O_3 ratio (Table 3.1). Hence gels with a high ratio of SiO_2/Al_2O_3 contain a low NaOH content, promoting the formation of high a SiO_2/Al_2O_3 zeolite due to the low relative solubility of the Al^{+3} ion with respect to the Si^{+4} ion in alkaline NaOH solutions. However, in this experiment, it was found that the maximum yield of ZSM-5 zeolite at 84% (w/w) was obtained at a SiO_2/Al_2O_3 ratio of 80, and that as the SiO_2/Al_2O_3 ratio increased above 80 then so the yield of the product tended to decrease. The Al_2O_3 content in the ZSM-5 attained from a high SiO_2/Al_2O_3 molar ratio ($\geq$ 400) might be too small to be detected by EDAX. According to Szostak[3], the pure silica polymorph of zeolite ZSM-5 was named 'Silicalite or Silicalite-1'.

The results summarized in Table 4.4 show that with increasing SiO_2/Al_2O_3 molar ratios, the surface area and the micropore volume of the product initially dramatically and dose-dependently increase and reach a maximum at a SiO_2/Al_2O_3 molar ratio of 200. Further increases in this molar ratio beyond 200, however, leads to a dose-dependent gradual decrease. This presumably resulted from crystal linkage leading to the forming of thin plates of aggregates. N_2 adsorption-desorption isotherms of calcined samples with SiO_2/Al_2O_3 molar ratios of 80-2075 were measured at -196 °C. They all revealed microporosity as a sharp knee at P/P_0 lower than 0.1 due to filling of micropores and capillary condensation as an adsorption hysteresis loop at higher P/P_0 which is characteristic of Type IV isotherms. As a representative, the N_2 adsorption-desorption isotherms and the pore size distribution curves of ZSM-5 with SiO_2/Al_2O_3 molar ratio of 80-2075 are shown in Fig. 4.10-4.16 and Fig. 4.17, respectively. The median pore radius

inferred from the curve is about 0.5 nm for the products obtained from SiO_2/Al_2O_3 molar ratios of 80-200, whilst those obtained from higher SiO_2/Al_2O_3 molar ratios of 400-2075 are slightly larger (~ 0.6 nm). The SEM micrographs of the hydrothermal products (Fig. 4.18) reveal the morphologies of the products at different SiO_2/Al_2O_3 molar ratios. The low SiO_2/Al_2O_3 molar ratios (<80) principally fragmented amorphous material and spheres of poorly crystalline zeolite were obtained, whist with higher SiO_2/Al_2O_3 molar ratios (≥80) well crystalline zeolite, with an average crystallite size 6-7 μm, was obtained. It was also clearly noticed that the crystalline ZSM-5 with a large surface area obtained from SiO_2/Al_2O_3 molar ratios of 80-800 have a round shaped crystal and is less aggregated, whist those obtained from the higher SiO_2/Al_2O_3 molar ratios (>800) are more tabular and strongly aggregated. The surface area of over 300 m^2/g is quite reasonable for the large sized and well-crystallized ZSM-5 (SiO_2/Al_2O_3 = 80-200) regarding to the previous reports.[5, 19, 77]

Table 4.4 The effect of varying the SiO_2/Al_2O_3 molar ratio on the BET surface area and the pore size of the obtained ZSM-5 zeolite and silicalite

SiO_2/Al_2O_3 molar ratio in the gel	BET surface area (m^2/g)	Micropore volume (cm^3/g)	Mesopore volume (cm^3/g)	Total pore volume (cm^3/g)
30	27	0.0059	0.0258	0.0358
50	82	0.0148	0.0254	0.0605
80	306	0.1050	0.0214	0.1454
100	308	0.1090	0.0306	0.1758
200	365	0.0962	0.0235	0.1871
400	215	0.0878	0.0343	0.1384
800	185	0.0660	0.0330	0.1264
1000	172	0.0390	0.0377	0.1264
2075	122	0.0166	0.0697	0.1241

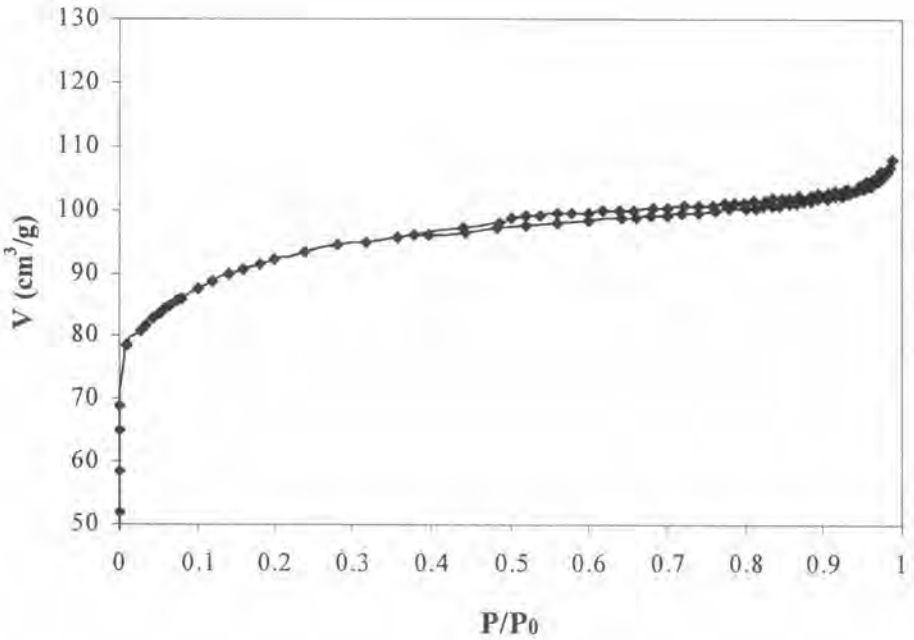

Fig. 4.10 Nitrogen adsorption-desorption isotherm of calcined ZSM-5 obtained at SiO_2/Al_2O_3 molar ratio of 80.

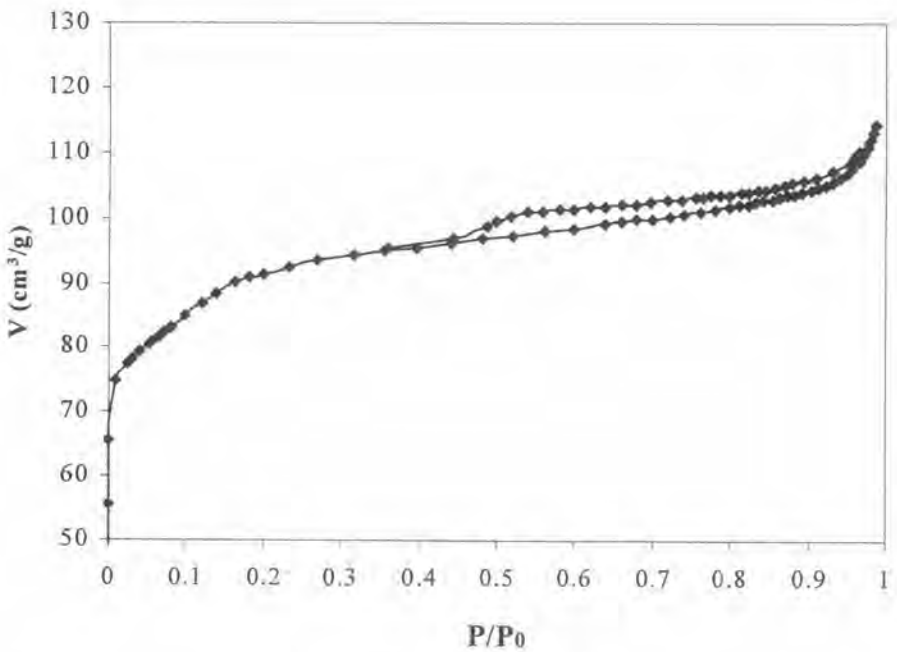

Fig. 4.11 Nitrogen adsorption-desorption isotherm of calcined ZSM-5 obtained at SiO_2/Al_2O_3 molar ratio of 100.

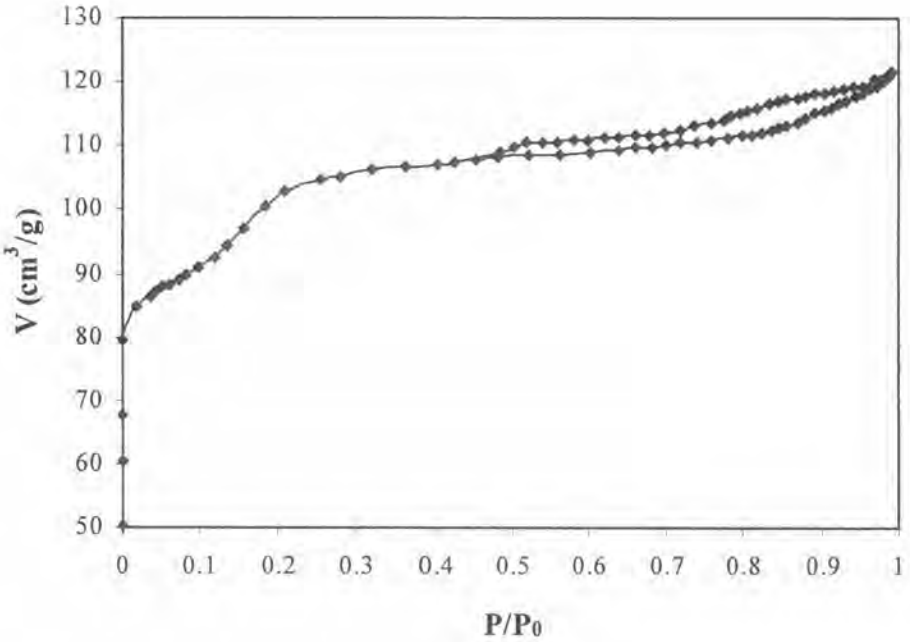

Fig. 4.12 Nitrogen adsorption-desorption isotherm of calcined ZSM-5 obtained at SiO_2/Al_2O_3 molar ratio of 200.

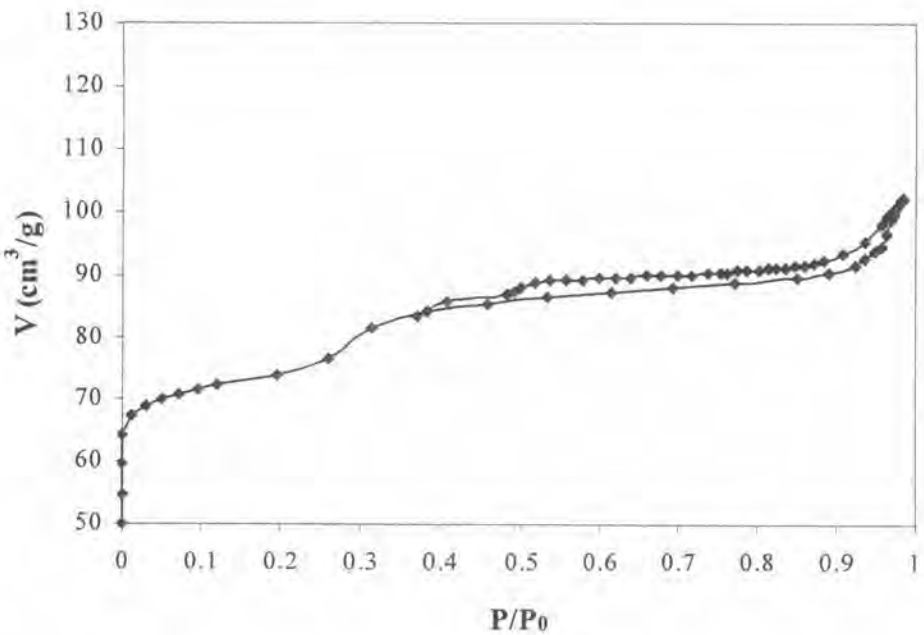

Fig. 4.13 Nitrogen adsorption-desorption isotherm of calcined ZSM-5 obtained at SiO_2/Al_2O_3 molar ratio of 400.

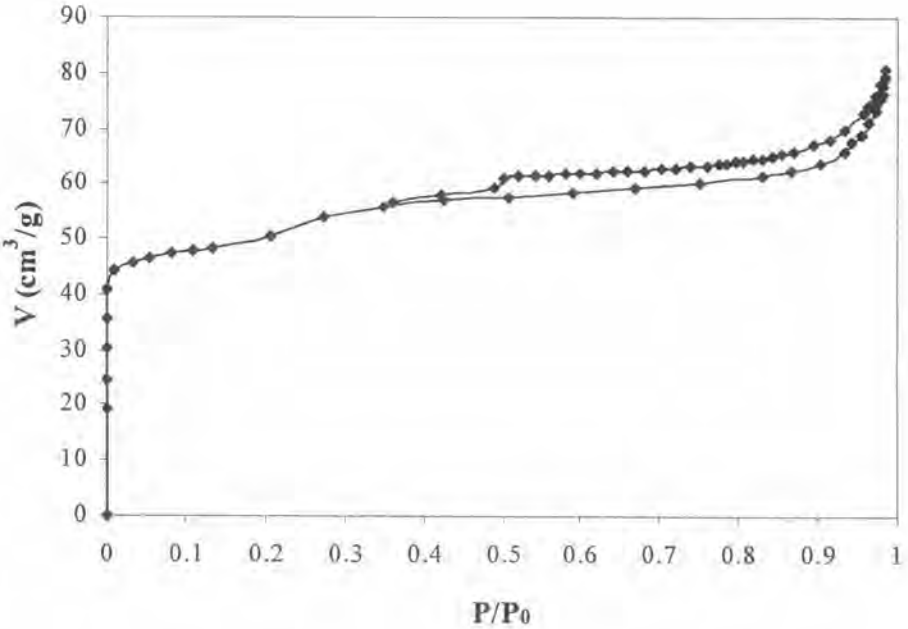

Fig. 4.14 Nitrogen adsorption-desorption isotherm of calcined ZSM-5 obtained at SiO_2/Al_2O_3 molar ratio of 800.

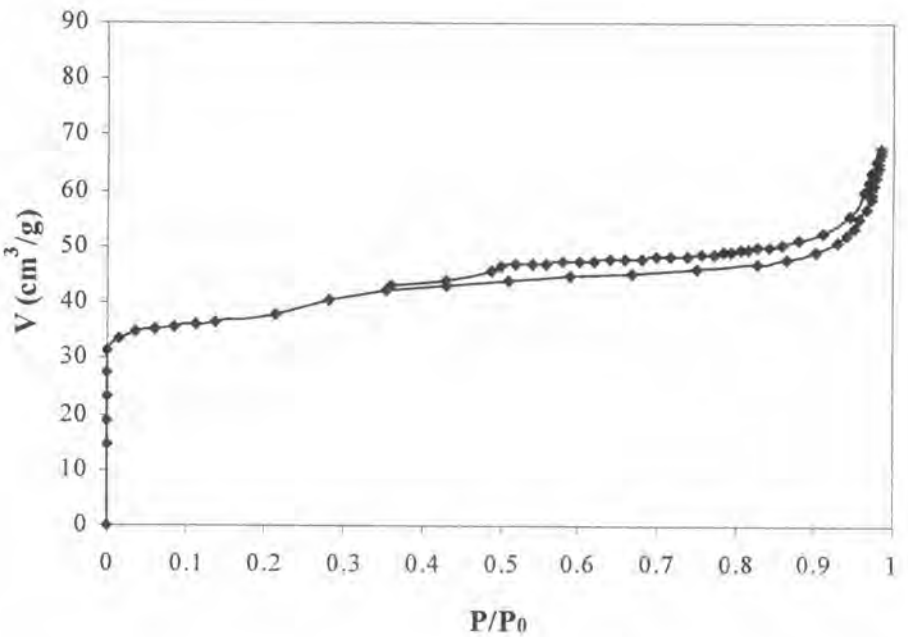

Fig. 4.15 Nitrogen adsorption-desorption isotherm of calcined ZSM-5 obtained at SiO_2/Al_2O_3 molar ratio of 1000.

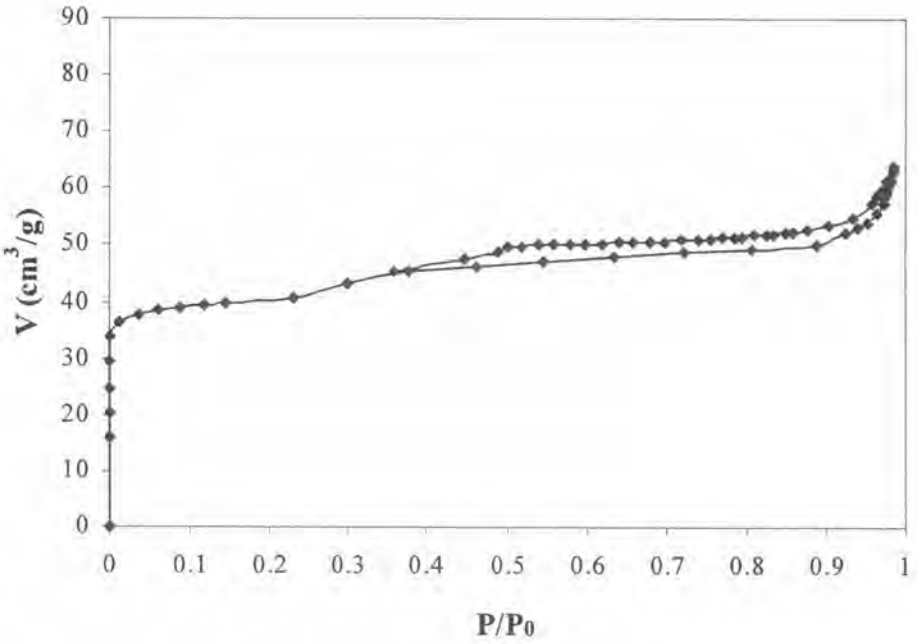

Fig. 4.16 Nitrogen adsorption-desorption isotherm of calcined ZSM-5 obtained at SiO_2/Al_2O_3 molar ratio of 2075.

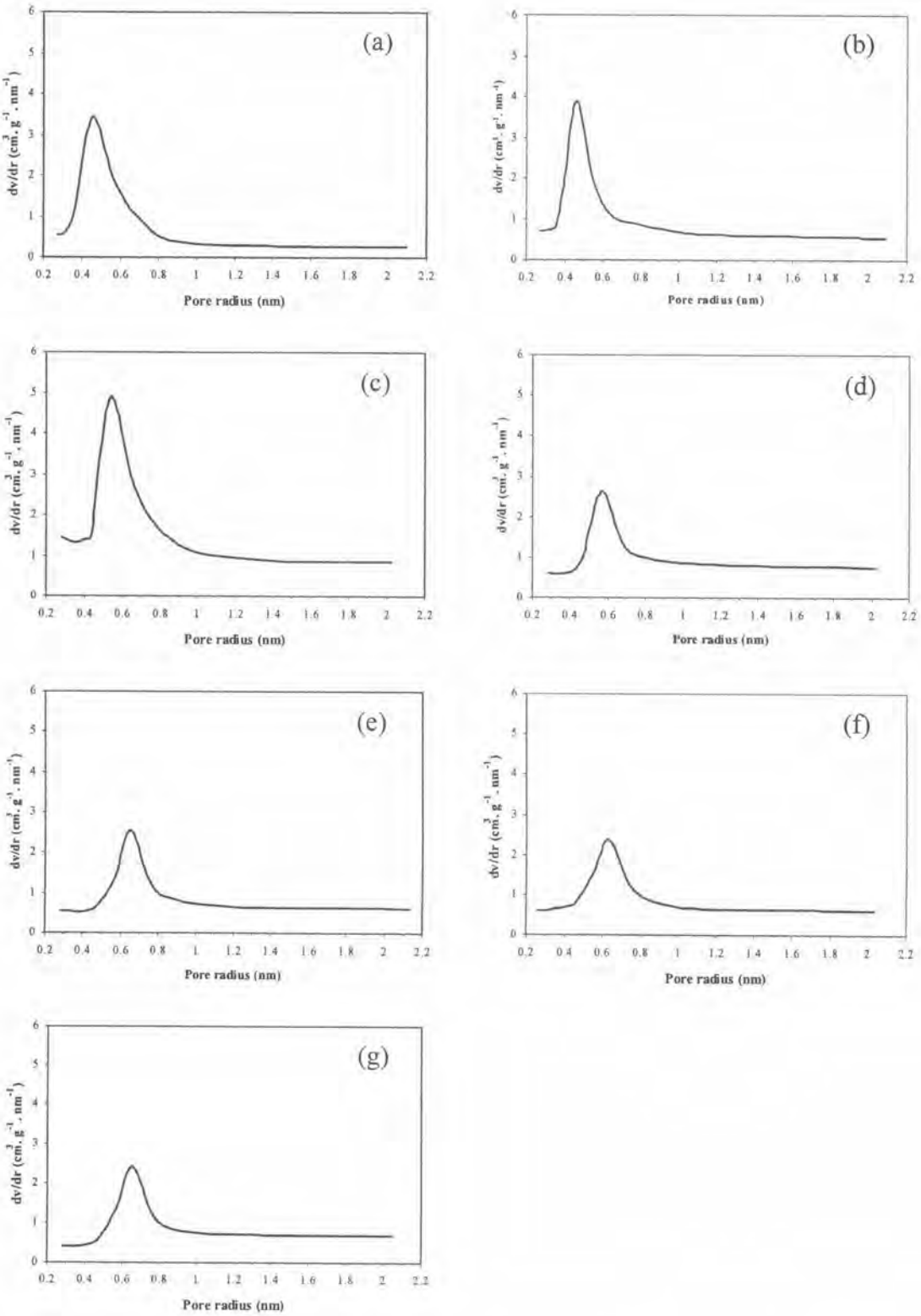

Fig. 4.17 Pore size distribution curve of ZSM-5 with different SiO_2/Al_2O_3 molar ratios of (a) 80 (b) 100 (c) 200 (d) 400 (e) 800 (f) 1000 and (g) 2075.

Infrared spectroscopy was also used to follow the effect of different SiO_2/Al_2O_3 molar ratios on the zeolitization process. Representative FT-IR spectra of the synthesized products after calcining, to get rid of the template, at 550 °C are shown in Fig. 4.19. According to Kordatos et al.[19] the vibration modes near 1100, 800 and 450 cm^{-1} are assigned to the internal vibrations of Si and AlO_4 tetrahedra in silica, quartz and cristobalite, respectively, whist the vibration modes near 550 and 1230 cm^{-1} are assigned to the double-ring tetrahedral vibration and asymmetric stretching of Si and AlO_4 tetrahedra in the zeolite framework, respectively. It is clearly seen that these vibration modes (internal and external) appear in all the synthesized samples but the characteristic vibration mode of the ZSM-5 framework at 1230 cm^{-1} is better resolved in the samples derived from SiO_2/Al_2O_3 molar ratios ranging from 80-200. This coincides with the transition of ZSM-5 zeolite to silicalite at a SiO_2/Al_2O_3 molar ratio of >200 (Table 4.3). It is worth noting that according to Szostak[3], the crystallization of ZSM-5 structure occurs over a wide range of SiO_2/Al_2O_3 molar ratios (from 15 to ∞) but that the SiO_2/Al_2O_3 molar ratio of 190 is the maximum ratio for an aluminosilicate to be defined as 'Zeolite'. Moreover, the sharpness and intensity of the absorption band near 550 cm^{-1} in the samples derived from a SiO_2/Al_2O_3 molar ratio of more than 80 confirm the high degree of crystallinity of ZSM-5 that was also revealed by XRD and SEM analyses. The bands at around 1600 cm^{-1}, attributed to the bending of molecular adsorbed water, revealed in the samples derived from a low SiO_2/Al_2O_3 molar ratio were also more clearly resolved in samples derived from SiO_2/Al_2O_3 molar ratios of 80 to 200. This indicates a high microporosity[78] which is in accordance with the results of surface area and micropore analyses presented in Table 4.4. In addition, the bands near 3652 and 3400 cm^{-1}, attributed to stretching vibrations of bulk silanol groups and molecular water OH^- groups and/or silanol group H ions, are present in the samples derived from SiO_2/Al_2O_3 molar ratios of 80 to 200, but only the band at around 3400 cm^{-1} persists throughout this range of samples. This indicates the reduction of Si-OH groups in the samples with SiO_2/Al_2O_3 molar ratios over 200.

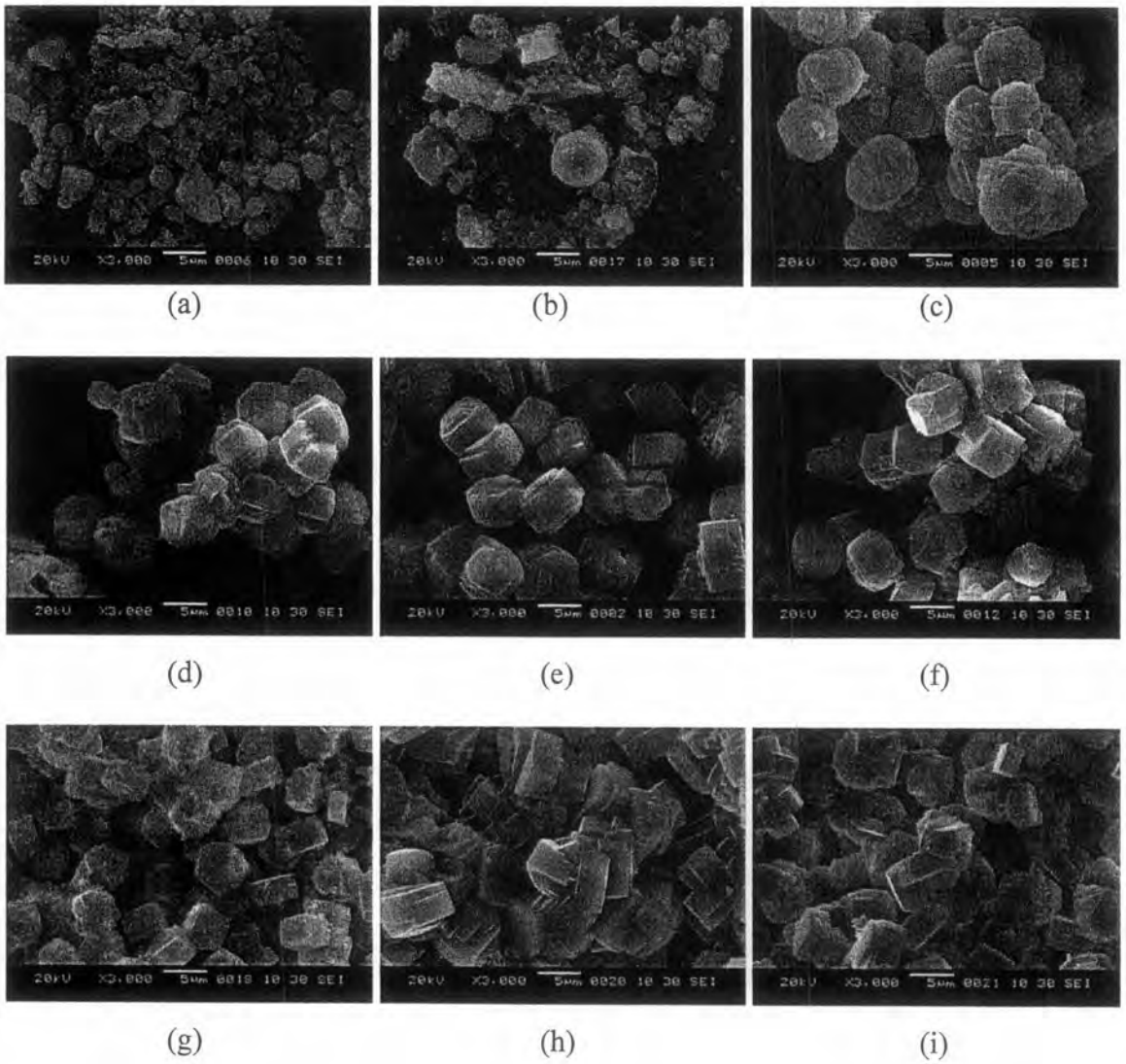

Fig. 4.18 Representative SEM micrographs of various as-synthesized ZSM-5 zeolites derived from SiO_2/Al_2O_3 molar ratios of (a) 30, (b) 50, (c) 80, (d) 100, (e) 200, (f) 400, (g) 800, (h) 1000 and (i) 2075.

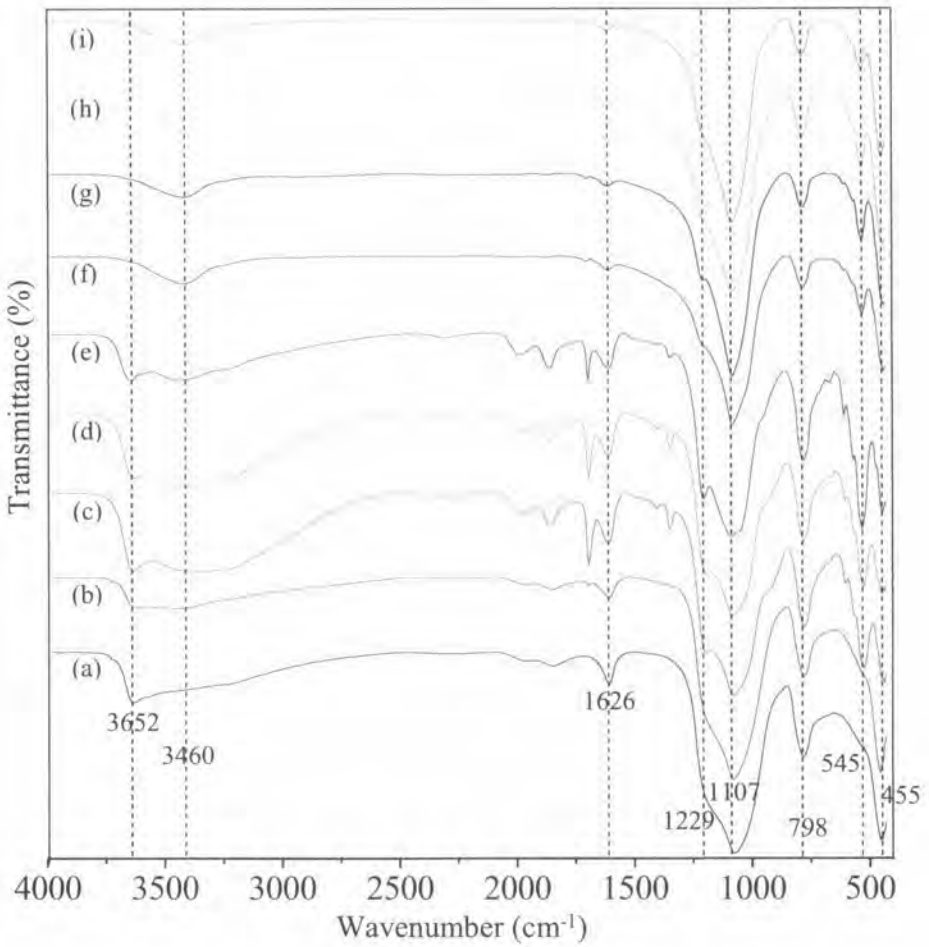

Fig. 4.19 Representative FT-IR spectra of calcined ZSM-5 derived from SiO_2/Al_2O_3 molar ratios of (a) 30, (b) 50, (c) 80, (d) 100, (e) 200, (f) 400, (g) 800, (h) 1000 and (i) 2075.

Preparation of TiO_2 powders and TiO_2/ZSM-5 composites

A. Characterization of the products

The values of specific surface area, rate constant for photocatalytic degradation and the content of Na_2SO_4 remaining on the calcined TiO_2 and the composite are presented in Table 4.5.

The rate constant of photocatalytic degradation was calculated up to a period of 2 h irradiation using the following equatuin[79]:

$$\ln C_0/C_t = kt$$

where C_0 and C_t represent the initial concentration of MB aqueous solution and the concentration measured at the irradiation time, t, respectively, and k represents the apparent rate constant.

The average crystal size of the powder was calculated from the full width at half maximum of anatase (101) in the XRD pattern (JCPDS No. 89-4921), using Scherrer's equation[80].

XRD patterns of TiO_2 powders calcined at different temperatures are shown in Fig. 4.20. The powders calcined at temperatures from 400 to 800 °C present pure anatase phase, showing an increase in the degree of crystallinity with crystal size increasing from 5 to 42 nm (Table 4.5). The result of phase analysis by XRD in Fig. 4.21 clearly revealed the poor crystalline anatase of TiO_2-1 powder and its coexistence in the composites. The FT-IR spectrum of TiO_2-1 in Fig. 4.22 shows an absorption peak of chemisorbed SO_4^{2-} at 1131 cm^{-1} and another large peak of the OH group at 3433 cm^{-1}, characteristics of sulfated TiO_2[81, 82]. It should be noted that the content of sulfate salt adsorbed on each sample of TiO_2 powder was too small to be detected by XRD but the white precipitate obtained after evaporating the collected washing waters on a hotplate was detectable by XRD as a mixture of two Na_2SO_4 salts (JCPDS No. 37-1465, thernardite (syn) and No. 24-1132, Na_2SO_4). Therefore, it was reasonable to assume that the excess sulfate ion on

TiO_2 particle was physically adsorbed as Na_2SO_4 salt. The SEM micrographs, Fig. 4.23, show that the particles of TiO_2-1 (~5 nm) only adhered to the surface of ZSM-5 and were not inside the pore (~5 Å).

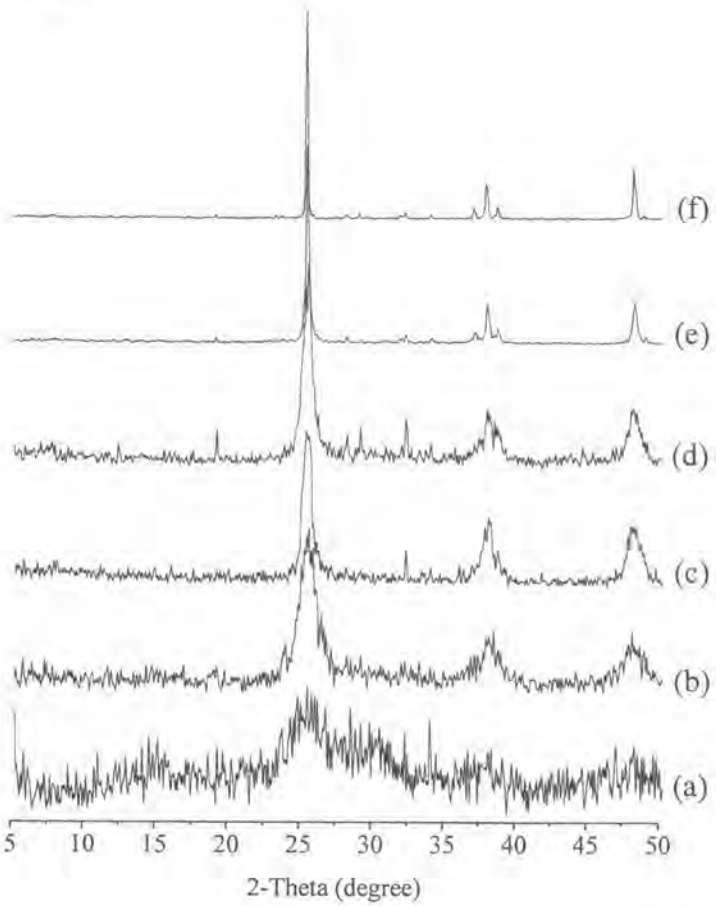

Fig. 4.20 XRD patterns of TiO_2 prepared at different calcinations temperatures: (a) as-prepared TiO_2, (b) 400 °C, (c) 500 °C, (d) 600 °C, (e) 700 °C and (f) 800 °C.

B. Photocatalytic activity of TiO_2 powders

The photocatalytic results of the TiO_2 powders synthesized at various conditions are presented in Fig. 4.24. The adsorption of dye in the dark of all the powders reached equilibrium at ~0.5 h. The absorbance in the dark by TiO_2-1 powder was high but under UV irradiation was very low, descending from TiO_2-1 to TiO_2-5 (crystalline anatase). From the preparation method, it was expected that some amount of SO_4^{2-} ion would

remain as Na_2SO_4 salt (water soluble and mp ~800 °C)[83] on the surface of TiO_2 particles. This sulfate salt ionized in the aqueous dye solution producing Na^+ and SO_4^{2-} ions. Most Na^+ ions would adsorb onto the weakly, negative charged surface of TiO_2 and few would diffuse away while the closely diffused SO_4^{2-} ions would act as bridging electrolyte that compressed the double layer of the TiO_2 sol[84] leading to the flocculation of the TiO_2 particles with the adsorbed dye in the dark and enhancing the subsequent photocatalysis. The absorbance in the dark of TiO_2-2 was approximately the same as TiO_2-1 but under UV irradiation was higher. Both absorbances of TiO_2-3 (sulfate-free) were the highest. The sequence of absorbance at 0.5 h UV irradiation was TiO_2-6 < TiO_2-5 < TiO_2-1 < TiO_2-4 < TiO_2-7 < TiO_2-2 < TiO_2-3 and TiO_2-6 ~P-25; TiO_2-1, TiO_2-4, TiO_2-5 ~ST-01. Obviously, the supportive effect of electrolyte in the adsorption mechanism of dye by TiO_2 powder was confirmed by the low catalytic rate of the washed and SO_4^{2-} -free TiO_2 powders (Table 4.5).

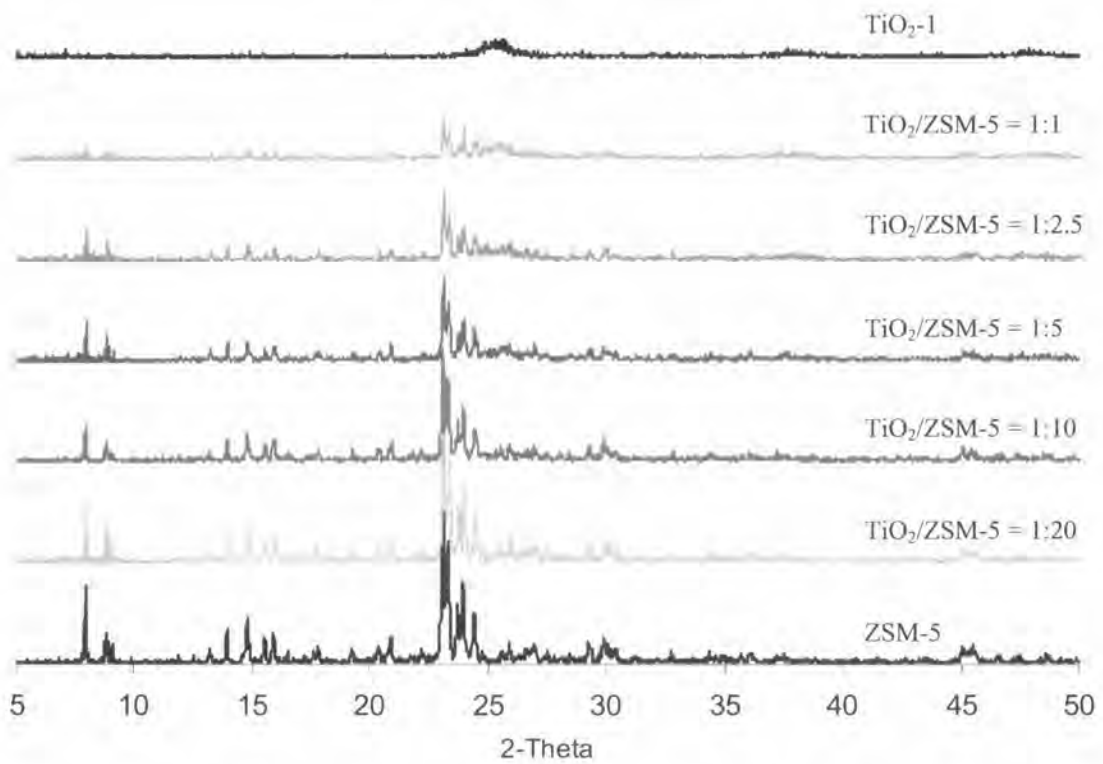

Fig. 4.21 XRD patterns of ZSM-5, TiO_2 and TiO_2/ZSM-5 composites.

(JCPDS No.42-0023 and 89-4921)

Table 4.5 BET surface area, apparent rate constant and content of adsorbed Na_2SO_4 of TiO_2, ZSM-5 and TiO_2/ZSM-5 composite

Sample, preparation condition (crystal size)	BET surface area (m^2/g)	k ($x10^{-2}$ h^{-1})	Na_2SO_4 (g/g powder or composite)
P-25 anatase/rutile	50	224	-
ST-01 anatase	300	105	-
TiO_2-1, 400 °C, filtered (5 nm, XRD)*	73	173	0.4780
TiO_2-2, 400 °C, washed with 50 ml distilled water (5.4 nm, XRD)	96	71	n.d.
TiO_2-3, 400 °C, sulfate-free (5.8 nm, XRD)	123	25	-
TiO_2-4, 500 °C, filtered (8.2 nm, XRD)	40	193	n.d.
TiO_2-5, 600 °C, filtered (10.3 nm, XRD)	32	198	n.d.
TiO_2-6, 700 °C, filtered (27 nm, XRD)	24	243	n.d.
TiO_2-7, 800 °C, filtered (42 nm, XRD)	5	93	n.d.
ZSM-5 (5 μm, SEM)	306	-	-
TiO_2/ZSM-5 = 1:20	306	41	0.0530
TiO_2/ZSM-5 = 1:10	294	73	0.0939
TiO_2/ZSM-5 = 1:5	260	111	0.1775
TiO_2/ZSM-5 = 1:2.5	247	19	0.2117
TiO_2/ZSM-5 = 1:1	212	-	0.3885

n.d. = not determined. It is understood that all the samples contains Na_2SO_4, except TiO_2-3, and it is assumed that TiO_2-1, TiO_2-4, TiO_2-5, TiO_2-6 and TiO_2-7 contain the same amount of Na_2SO_4 but there is lesser amount in TiO_2-2.

*TiO_2-1 was employed in the preparation of all the composites due to its large surface area and residual SO_4^{2-} content.

C. Photocatalytic activity of TiO_2/ZSM-5 composites

Since, $TiOSO_4$ and NaOH were used as the sources of TiO_2 and the hydrolyzing agent, respectively, it was expected that there would be some trace of Na_2SO_4 on the surface of the filtered TiO_2/ZSM-5 composites as well as on the TiO_2 powder after calcining. This expectation was confirmed by the detection of chemically adsorbed SO_4^{2-} (Fig. 4.22). The content of Na_2SO_4 adsorbed on TiO_2-1 powder was ~0.478 g/g powder or composite (Table 4.5). Those on the composites were dependent on the adsorbed TiO_2 content. From the results shown in Fig. 4.25, in the dark, the adsorption of dye by ZSM-5

and composites reached equilibrium at ~0.5 h and that of ZSM-5 was nearly the same after UV irradiation. Adsorption limit is characteristic of a particular material and related to its surface area which can be tailored if the material is made into a composite, and in the presence Na_2SO_4 the mechanism of adsorption is more complicated. At low TiO_2 loadings (wt ratio of TiO_2/ZSM-5 = 1:20, 1:10 and 1:5), the surface areas of 1:20 and 1:10 composites were not much different from those of ZSM-5 (Table 4.5). Therefore the absorbance in the dark was close to that of the ZSM-5, but the photocatalysis under UV irradiation depended on the TiO_2 content and close contact between the adsorbed dye and TiO_2 particles, hence the higher TiO_2 composite showed lower absorbance under UV irradiation. At 1:5 TiO_2 loading, there was an optimal synergy of Na_2SO_4 content and surface area of the composite resulting in the highest catalytic rate. On the contrary, at 1:2.5 TiO_2 loading, the surface area of the composite was ~3/4 of ZSM-5 and the exposed surface of ZSM-5 was large enough to exhibit the neutralization effect of Na^+ ion[85]. The composite became less negative, therefore, the dye adsorption in the dark was low, leading to high absorbance and the lowest catalytic rate. From this point and beyond, the content of TiO_2 was the main factor that controlled the mechanism.

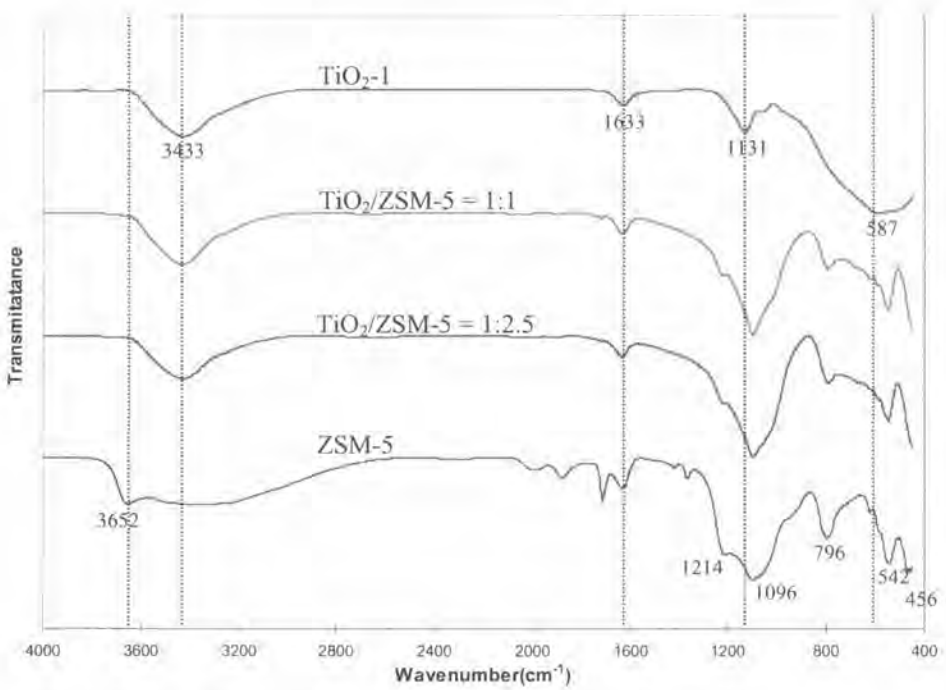

Fig. 4.22 FT-IR spectra of ZSM-5, TiO_2 and TiO_2/ZSM-5 composites.

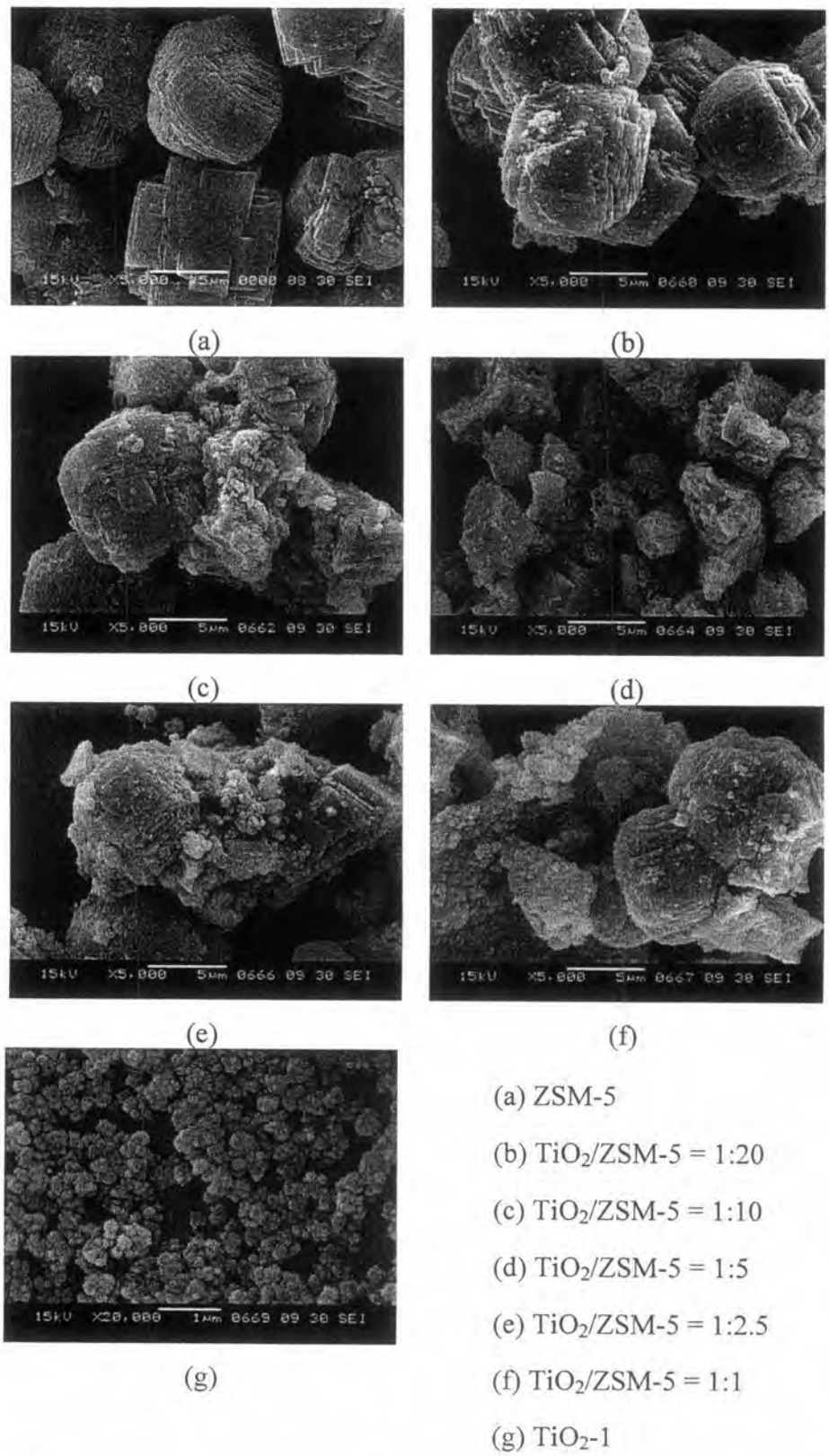

(a) ZSM-5

(b) TiO_2/ZSM-5 = 1:20

(c) TiO_2/ZSM-5 = 1:10

(d) TiO_2/ZSM-5 = 1:5

(e) TiO_2/ZSM-5 = 1:2.5

(f) TiO_2/ZSM-5 = 1:1

(g) TiO_2-1

Fig. 4.23 SEM micrographs of ZSM-5, TiO_2 and TiO_2/ZSM-5 composites.

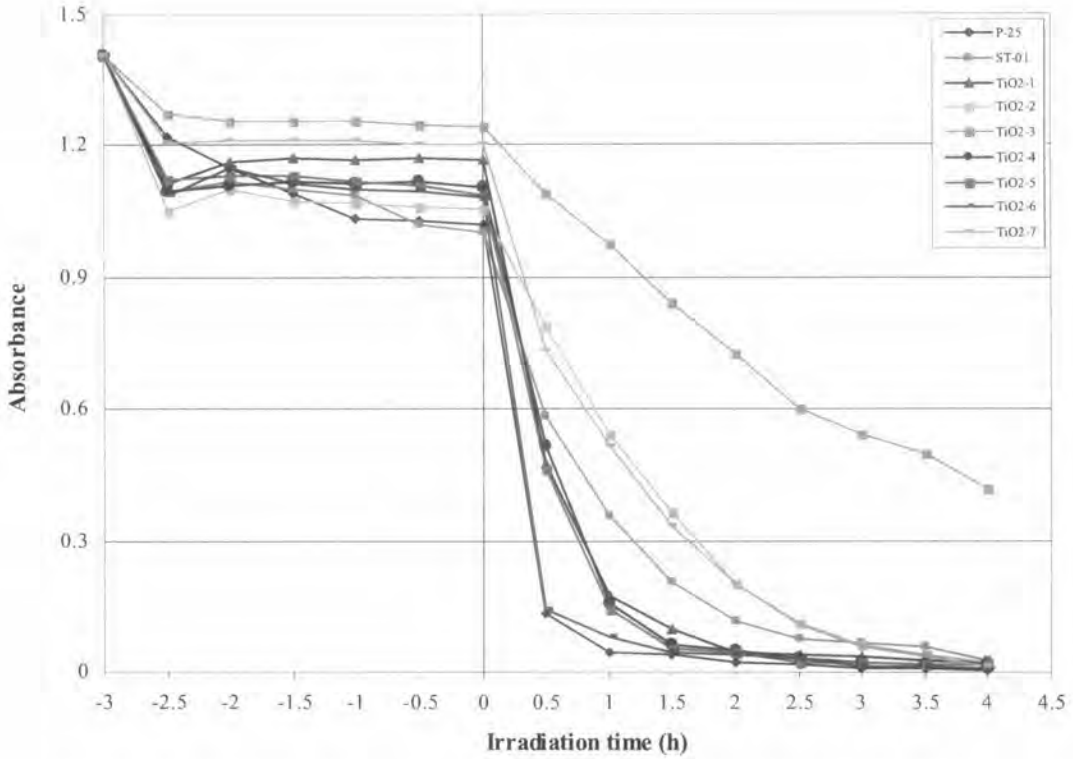

Fig. 4.24 Photocalytic results of commercial TiO_2 and synthesized TiO_2.

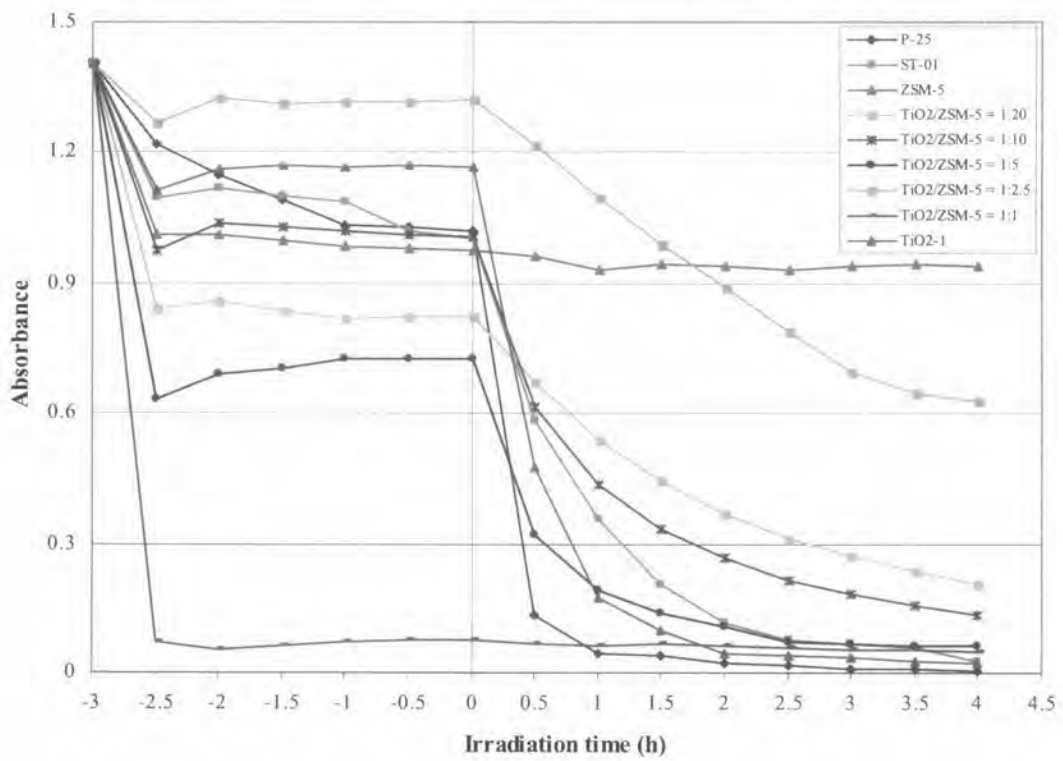

Fig. 4.25 Photocatalytic activities of TiO_2 powder and TiO_2/ZSM-5 composites.

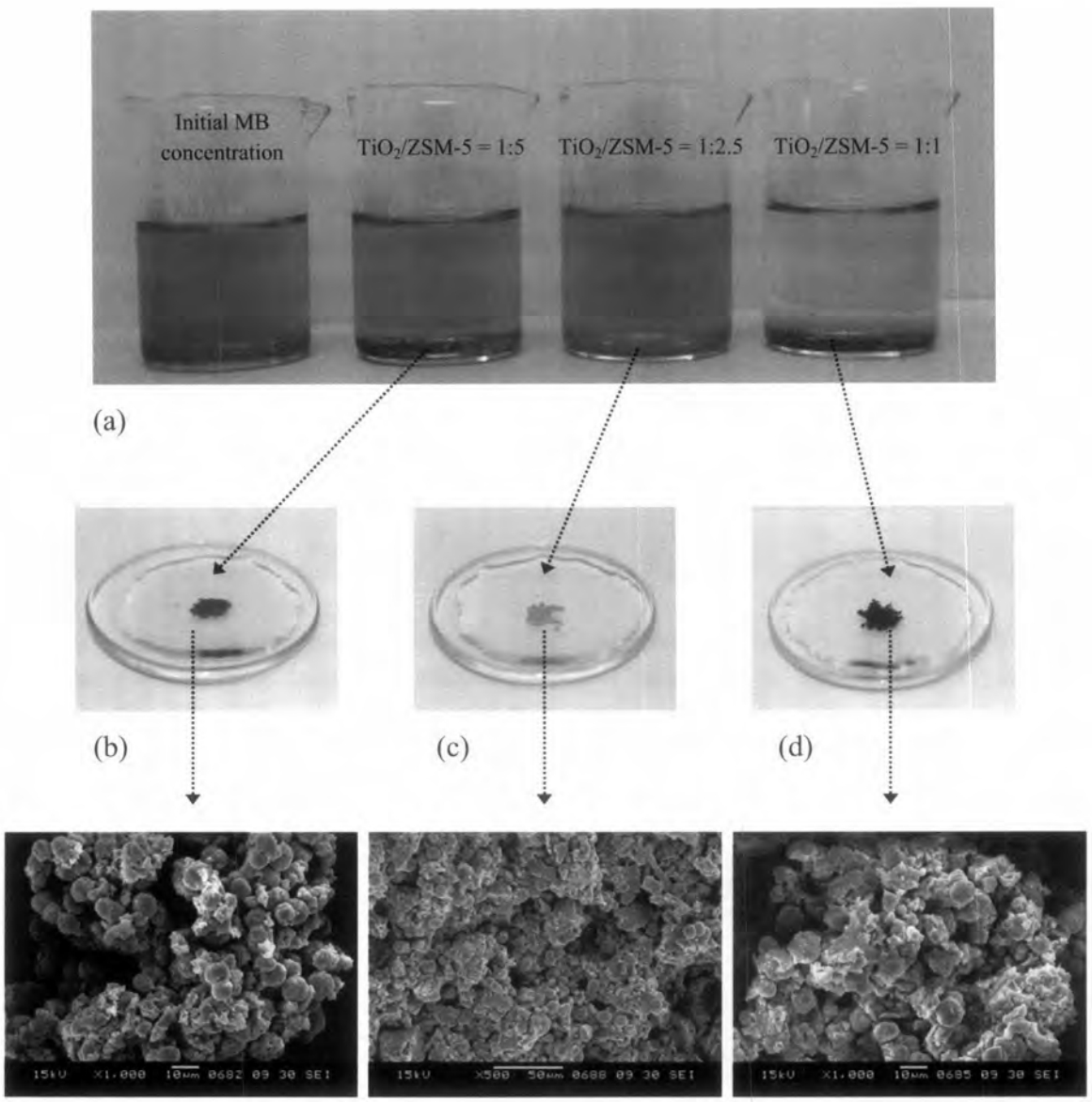

Fig. 4.26 Photographs of (a) MB adsorption of the composite in the dark and the settled flocs in MB solution containing 0.01 g of (b) TiO_2/ZSM-5 = 1:5 (c) TiO_2/ZSM-5 = 1:2.5 (d) TiO_2/ZSM-5 = 1:1 and SEM imcrographs (e-g) of the settled flocs (air dry) from (b), (c) and (d).

It was noticed that for 1:20 to 1:2.5 TiO_2 loadings, composite particles in the dye solution were in a state of suspension after 0.5 h in the dark and took a few hours to settle. For 1:1 TiO_2 loading, the surface area of the composite was ~2/3 of ZSM-5, and the content of ZSM-5 was small (half of ZSM-5) so each composite particle contained quite an amount of Na_2SO_4, hence the flocculating concentration of Na_2SO_4 was reached. Consequently, the contacts between TiO_2 particles were enhanced through the powerful flocculation of the ionized Na_2SO_4 resulting in the forming of loose large flocs of the composite particles. The dye adsorption onto the composites was continuously enhanced by the additional capillary action of the flocs which, on the removal of magnetic stirring, fell down to the bottom of the breaker. Accordingly, all the dye was almost physically adsorbed, and the solution became clear while the settled flocs became deep blue (Fig. 4.26). The bleaching of the dye solution in the dark was instantaneous and the absorbance dropped to almost zero within 0.5 h. Consequently, the oxidation of the dye under UV irradiation went on with a gradual change in the absorbance of the dye solution. After 2.5 h, the solutions with 1:5 and 1:1 TiO_2 loadings were colorless and the flocs at bottom were lighter in color. Fig. 4.27 is schematic model proposed for 1:1 TiO_2 loading showing that most of the ionized Na^+ would leave TiO_2 and readily adsorb onto the exposed surface of ZSM-5 because of its stronger negative charged surface leading to neutralization, and an exposed negative charged surface of TiO_2. It can be said that the mechanism of adsorption of dye in the dark by the composite was the interaction of both the exposed surface of ZSM-5 and TiO_2 content. The low absorbance in the dark meant that a high dye content was adsorbed, leading to a better and larger interface contact between the dye and TiO_2 particles, and hence faster oxidation of the dye under UV irradiation.

Therefore the mechanism of the oxidation of the dye by the composite under UV irradiation directly depended on the weight ratio of TiO_2 loading. The optimal weight ratio of TiO_2 loading, taken as the point of optimal interaction between the exposed surface of ZSM-5 and that of TiO_2, judging from the adsorption in the dark and the catalytic reaction at 0.5 h after UV irradiation was 1:5 TiO_2 loading.

In the case of TiO_2 powders, P-25 and ST-01, it was clear that the mechanisms of adsorption and oxidation of the dye were different from those of the composites. The

surface area of the powder accounted for both mechanisms. The better catalytic action of P-25 (50 m^2/g) over that of ST-01 which has a finer particle size, to a certain extent, may also be supported by its phase composition and slow electron-hole recombination[86]. The ratio of rutile/anatase is about 30/70 in P-25, while ST-01 is 100% large surface area (~300 m^2/g) anatase. For sample, TiO_2-1, the photocatalytic action was greatly assisted by the effective content of Na_2SO_4 electrolyte. However, unlike the case of composites whose particle size was much larger, in TiO_2-1 powder only small particles of flocs were formed and retained suspended in the solution.

However, besides the sulfate (SO_4^{2-}) content and the effect of TiO_2/ZSM-5 composite, the photocatalytic activities of our TiO_2 powder could also be improved by increasing its crystallinity through higher temperature calcining as seen in Fig. 4.24 It seemed that the larger particle size or the better crystallinity of TiO_2 enhanced the early catalytic reaction under UV irradiation. However, the rates at 2.5 h of 400-500 °C samples were not much different. The surface area of TiO_2 at 700 °C was 24 m^2/g (Table 4.5) and gave the best catalytic reaction with the highest rate at 0.5 h, while the adsorption of dye in the dark was almost the same for all the samples, excluding the SO_4^{2-}-free (TiO_2-3).

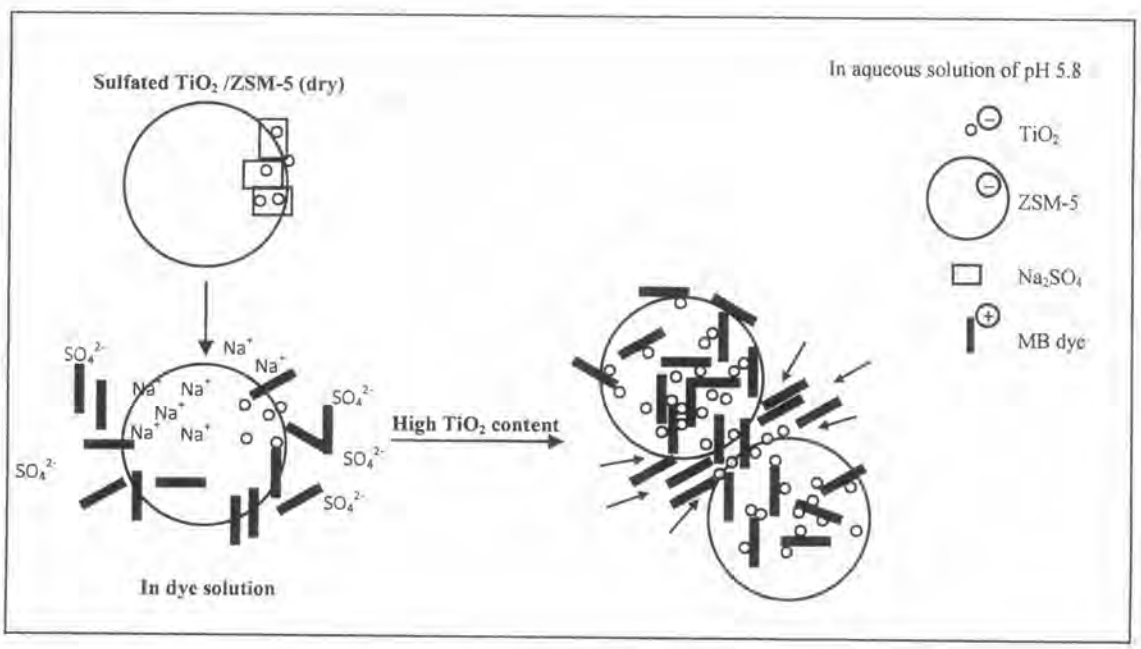

Fig. 4.27 Schematic model of the interaction.